Inorganic Chemistry

Article

pubs.acs.org/IC

Rare-Earth Manganese Copper Phosphides $REMnCu_4P_3$ (RE = Gd–Ho): The First Quaternary Ordered Variants of the YCo_5P_3-Type Structure

Krishna K. Ramachandran, Stanislav S. Stoyko, C. Scott Mullen, and Arthur Mar*

Department of Chemistry, University of Alberta, Edmonton, Alberta, Canada T6G 2G2

Supporting Information

ABSTRACT: The quaternary rare-earth phosphides $REMnCu_4P_3$ (RE = Gd–Ho) were obtained from direct reactions of the elements at 800 °C. They are the first examples in which ordering of two different transition-metal atoms takes place within the orthorhombic YCo_5P_3-type structure [Pearson symbol *oP*36, space group *Pnma*, $Z = 4$; $a = 12.667(2)$–$12.6489(4)$ Å, $b = 3.8119(7)$–$3.7755(1)$ Å, and $c = 10.895(2)$–$10.8632(4)$ Å for RE = Gd–Ho]. Columns of trigonal prisms centered by P atoms are connected in propellor-shaped units in zigzag arrangements to generate square-pyramidal (CN5) sites that are occupied by Mn atoms and tetrahedral sites (CN4) that are occupied by Cu atoms. Spin-polarized band-structure calculations predict that the hypothetical compound $YMnCu_4P_3$ will exhibit magnetic ordering. Electrical resistivity measurements on $TbMnCu_4P_3$ indicate a poor metal.

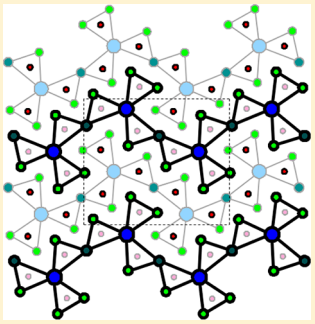

INTRODUCTION

A large number of ternary rare-earth transition-metal pnictides RE–M–Pn, mostly phosphides, have a metal-to-nonmetal ratio equal or close to 2:1, an indication of their close structural relationship to metal-rich binary pnictides M_2Pn.[1−3] These binary and ternary pnictides are attractive for their applications in catalysis (e.g., hydrodesulfurization and hydrodenitrogenation by Ni_2P and its ternary derivatives)[4,5] and their exotic magnetic properties (e.g., unconventional quantum criticality in $RE_2M_{12}P_7$).[6] These compounds share a common motif of Pn-centered trigonal prisms, which can be connected in many different ways to generate several homologous series of structure types.[1−3] One extensive branch of hexagonal structures has the general formula $RE_{n(n-1)}M_{(n+1)(n+2)}Pn_{n(n+1)+1}$, whose members exhibit increasingly larger triangular assemblies of these trigonal prisms: Fe_2P ($n = 1$), $Zr_2Fe_{12}P_7$ ($n = 2$), $Zr_6Ni_{20}P_{13}$ ($n = 3$), and $(La,Ce)_{12}Rh_{30}P_{21}$ ($n = 4$). A shorter branch of orthorhombic structures has the general formula $RE_{n(n-1)}M_{(n+1)(n+2)-2}Pn_{n(n+1)}$ and contains the same types of triangular assemblies but arranged in zigzag chains: Co_2P ($n = 1$) and YCo_5P_3 ($n = 2$). The metal atoms can occupy up to four possible types of coordination environments: trigonal prisms (CN6), square pyramids (CN5), tetrahedra (CN4), and trigonal planes (CN3). In accordance with the relative sizes of these sites, the general trend is that rare-earth metal atoms occupy CN6 sites, group 4 metal atoms occupy CN6 and CN5 sites, and the remaining transition-metal atoms occupy CN5, CN4, and CN3 sites. The variety of available sites offers the possibility of site ordering when several types of metals having different sizes and coordination preferences are introduced. Although there are now hundreds of such ternary pnictides that demonstrate the viability of this principle, to date there have been very few examples of quaternary pnictides. Following up on an earlier report of the quaternary mixed-metal pnictides $RE_2M_3M'_9Pn_7$ (M = Cr, W; M′ = Fe, Co; Pn = P, As) for which only cell parameters were provided,[7] we recently prepared the series $RE_2Mn_3Cu_9Pn_7$ (Pn = P, As) and confirmed that they adopt an ordered variant of the hexagonal $Zr_2Fe_{12}P_7$-type structure.[8] With this initial success, we wondered whether complex metal ordering could also be introduced into the orthorhombic branch of these 2:1 phases. The closest related example, with a metal-to-nonmetal ratio of slightly less than 2:1, is $LaZr_2Ni_4As_4$, which has a monoclinic structure resembling that of orthorhombic YCo_5P_3.[9]

Herein we present the synthesis and characterization of the series of rare-earth manganese copper phosphides $REMnCu_4P_3$, which are the first examples of quaternary ordered derivatives of the YCo_5P_3-type structure. The electronic structure of the hypothetical compound $YMnCu_4P_3$ was examined, and the electrical resistivity of $TbMnCu_4P_3$ was measured.

EXPERIMENTAL SECTION

Synthesis. Starting materials were freshly filed RE pieces (99.9%, Hefa), Mn powder (99.6%, Alfa-Aesar), Cu powder (99.8%, Alfa-Aesar), and red P powder (99.9%, Alfa-Aesar). In the course of reactions intended to prepare $RE_2Mn_3Cu_9P_7$ (which forms for RE = La–Nd, Sm, Gd–Dy), other quaternary phases with slightly different compositions were formed for the later RE components starting from Gd, which were subsequently identified to be $REMnCu_4P_3$. Thus, mixtures of the elements in this precise stoichiometry, on a 0.3-g scale, were pressed into pellets and loaded into fused-silica tubes, which were evacuated, sealed, and heated at 800 °C for 10 days. To promote

Special Issue: To Honor the Memory of Prof. John D. Corbett

Received: August 27, 2014
Published: October 28, 2014

crystal growth, the products of these reactions were reground, pressed into pellets, and subjected to the same heat treatment again in the presence of about 30 mg of I_2, which acts as a mineralizing agent. Analysis by powder X-ray diffraction (XRD), performed with Cu Kα_1 radiation on an Inel diffractometer equipped with a curved position-sensitive detector (CPS 120), revealed that the samples generally consisted of not more than ~50% $REMnCu_4P_3$. It was difficult to obtain phase-pure samples of $REMnCu_4P_3$ because of the closeness of their compositions to those of the competing quaternary phases $RE_2Mn_3Cu_9P_7$, which were often found in smaller amounts in the samples, along with binary phosphides; this is a common problem in the synthesis of other metal-rich phases with a metal-to-nonmetal ratio of 2:1.[10] The range of RE substitution was found to be limited to Gd–Ho. The corresponding arsenides did not form under the synthetic conditions above. Attempts were also made to elucidate the possibility of a solid solution $RE(Mn_xCu_{1-x})_5P_3$ (RE = Tb, Ho; x = 0–1 in increments of 0.2). The limiting all-copper member $RECu_5P_3$ (x = 0) did not form. At x = 0.2, formation of the title compounds $REMnCu_4P_3$ was confirmed but in conjunction with the competing phase $RE_2Mn_3Cu_9P_7$. At x = 0.4, the products consisted of the slightly Mn-richer phase $RE_2Mn_3Cu_9P_7$, along with small amounts of binary RE–P and Cu–P phases. These results indicate that $REMnCu_4P_3$ and $RE_2Mn_3Cu_9P_7$ are in equilibrium with each other and connected through a tie-line in the complex quaternary phase diagram. Given the increments in x used in this study, any phase width would be narrow [i.e., $RE(Mn_{0.2(1)}Cu_{0.9(1)})_5P_3$]. Energy-dispersive X-ray (EDX) analysis on crystals of $REMnCu_4P_3$ was carried out on a JEOL JSM-6010LA scanning electron microscope, indicating reasonable agreement with expectations (Table S1 in the Supporting Information, SI). However, distinguishing between crystals of $REMnCu_4P_3$ and $RE_2Mn_3Cu_9P_7$ was challenging because of their similar needle-shaped habits and chemical compositions. Ultimately, single-crystal XRD experiments were essential to confirm their identity.

Structure Determination. Intensity data were collected at −100 °C on a Bruker PLATFORM diffractometer equipped with a SMART APEX II CCD area detector and a graphite-monochromated Mo Kα radiation source, using ω scans in 5–8 batches at different ϕ angles with a frame width of 0.3° and an exposure time of 15 or 20 s/frame. Face-indexed numerical absorption corrections were applied. Structure refinements were carried out with use of the *SHELXTL* (version 6.12) program package.[11] The centrosymmetric orthorhombic space group *Pnma* was chosen on the basis of Laue symmetry and intensity statistics. Direct methods revealed all initial atomic positions, which were standardized with the program *STRUCTURE TIDY*.[12] Among the five metal sites available, one was occupied by Mn atoms and four by Cu atoms. This ordered model was confirmed by refinements in which each site was allowed to be occupied by a mixture of Mn and Cu atoms with no restriction placed on the overall composition. In $GdMnCu_4P_3$, for example, the nominal Mn site contained 0.89(2) Mn and 0.11(2) Cu, whereas the four nominal Cu sites contained 0.00(2)–0.05(2) Mn and 0.95(2)–1.00(2) Cu. The Mn site consistently exhibited higher displacement parameters than the Cu sites. However, when the occupancy of this site was freely refined, it converged to 1.03(1) Mn in $GdMnCu_4P_3$. Elevated displacement parameters for this site are observed in other YCo_5P_3-type structures and are likely inherent to its higher coordination (CN5).[13] After final refinements, agreement factors were acceptable and difference electron density maps were featureless. Abbreviated crystallographic data are listed in Table 1, atomic coordinates and displacement parameters in Table 2, and selected interatomic distances in Table 3. Full crystallographic details are listed in Table S2 in the SI, and further data in the form of crystallographic information files (CIFs) are available as SI.

Band-Structure Calculation. Tight-binding linear-muffin-tin orbital band-structure calculations were performed within the local density and atomic spheres approximation with use of the Stuttgart *TB-LMTO-ASA* program (version 4.7).[14] To avoid computational difficulties associated with 4f orbitals, a hypothetical model $YMnCu_4P_3$ containing a nonmagnetic RE component was considered. The basis set consisted of Y 5s/5p/4d/4f, Mn 4s/4p/3d, Cu 4s/4p/3d, and P 3s/3p/3d orbitals, with the Y 5p/4f and P 3d orbitals being downfolded. Integrations in reciprocal space were carried out with an improved tetrahedron method over 576 irreducible k points within the first Brillouin zone. The calculations were repeated with spin polarization included.

Table 1. Crystallographic Data for $REMnCu_4P_3$ (RE = Gd–Ho)

	$GdMnCu_4P_3$	$TbMnCu_4P_3$	$DyMnCu_4P_3$	$HoMnCu_4P_3$
fw (amu)	559.26	560.93	564.51	566.94
space group	*Pnma* (No. 62)	*Pnma* (No. 62)	*Pnma* (No. 62)	*Pnma* (No. 62)
a (Å)	12.667(2)	12.6535(4)	12.6485(4)	12.6489(4)
b (Å)	3.8119(7)	3.7955(1)	3.7841(1)	3.7755(1)
c (Å)	10.895(2)	10.8761(3)	10.8680(3)	10.8632(4)
V (Å^3)	526.05(17)	522.34(3)	520.18(3)	518.78(3)
Z	4	4	4	4
T (K)	173	173	173	173
ρ_{calcd} (g/cm^3)	7.061	7.133	7.208	7.259
λ (Å)	0.71073	0.71073	0.71073	0.71073
μ(Mo Kα) (mm^{-1})	31.38	32.45	33.35	34.29
$R(F)$ for $F_o^2 > 2\sigma(F_o^2)^a$	0.019	0.020	0.022	0.016
$R_w(F_o^2)^b$	0.046	0.045	0.051	0.035

$^aR(F) = \sum||F_o| - |F_c||/\sum|F_o|$. $^bR_w(F_o^2) = [\sum[w(F_o^2 - F_c^2)^2]/\sum wF_o^4]^{1/2}$; $w^{-1} = [\sigma^2(F_o^2) + (Ap)^2 + Bp]$, where $p = [\max(F_o^2,0) + 2F_c^2]/3$.

Electrical Resistivity. From a relatively long crystal (~1 mm) of $TbMnCu_4P_3$, a small fragment was cut off and confirmed by single-crystal XRD to be the desired phase. The remainder of this crystal was mounted for standard four-probe electrical resistivity measurements, made between 2 to 300 K on a Quantum Design Physical Property Measurement System equipped with an alternating-current transport controller (model 7100). The current was 100 μA, and the frequency was 16 Hz. The measurement was repeated twice on this sample and was reproducible on a second sample.

RESULTS AND DISCUSSION

The quaternary rare-earth phosphides $REMnCu_4P_3$ could be obtained by reactions of the elements at 800 °C for later RE members (Gd–Ho), whose unit cell volumes decrease regularly in accordance with the lanthanide contraction (Figure 1). There was no evidence for the existence of any significant solid solution in $RE(Mn_xCu_{1-x})_5P_3$, and the hypothetical end members $REMn_5P_3$ and $RECu_5P_3$ are unknown. They are the first well-characterized examples of quaternary ordered representatives of the orthorhombic YCo_5P_3-type structure.[13] Previous examples of this structure type were restricted to ternary phases, mostly phosphides ($REFe_5P_3$, $RECo_5P_3$, $ThFe_5P_3$, and UMn_5P_3)[10,13,15−19] but also a few arsenides (YCo_5As_3),[20] germanides ($TbMn_5Ge_3$),[21] and indides [AMg_5In_3 (A = Sr, Ba) and $Ca_2Au_3In_4$ having a different site ordering].[22,23] The possibility for more complex ordering was already suggested with the initial discovery of YCo_5P_3 itself several decades ago (through the proposal of a compound such as $YRhCo_4P_3$), but no evidence had been forthcoming.[13] Site ordering in the closely related hexagonal $Zr_2Fe_{12}P_7$-type structure was recently demonstrated in the quaternary phosphides $RE_2Mn_3Cu_9P_7$, which forms for a much wider range of RE members (La–Nd, Sm, and Gd–Dy).[8] In fact, these two types of quaternary phases are often found together during synthesis, and as has been noted previously, it is difficult in general to obtain single-phase samples of YCo_5P_3- or

dx.doi.org/10.1021/ic502075x | *Inorg. Chem.* 2015, 54, 860–866

Table 2. Atomic Coordinates and Equivalent Isotropic Displacement Parameters for $REMnCu_4P_3$ (RE = Gd−Ho)

atom[a]	x	y	z	U_{eq} (Å^2)[b]
$GdMnCu_4P_3$				
Gd	0.29164(2)	$^1/_4$	0.92055(2)	0.00530(7)
Mn	0.01802(6)	$^1/_4$	0.79141(7)	0.01327(14)
Cu1	0.00524(4)	$^1/_4$	0.41028(5)	0.00772(11)
Cu2	0.06429(4)	$^1/_4$	0.03921(5)	0.00705(11)
Cu3	0.30501(4)	$^1/_4$	0.62889(5)	0.00761(11)
Cu4	0.32212(4)	$^1/_4$	0.21645(5)	0.00740(11)
P1	0.11478(8)	$^1/_4$	0.59499(10)	0.00540(18)
P2	0.13005(8)	$^1/_4$	0.24297(10)	0.00564(18)
P3	0.37862(8)	$^1/_4$	0.42212(9)	0.00525(18)
$TbMnCu_4P_3$				
Tb	0.29139(2)	$^1/_4$	0.92061(2)	0.00559(7)
Mn	0.01840(6)	$^1/_4$	0.79065(7)	0.01336(14)
Cu1	0.00499(4)	$^1/_4$	0.41080(5)	0.00792(11)
Cu2	0.06430(4)	$^1/_4$	0.03966(5)	0.00730(11)
Cu3	0.30535(4)	$^1/_4$	0.62915(5)	0.00781(11)
Cu4	0.32170(4)	$^1/_4$	0.21628(5)	0.00761(11)
P1	0.11560(8)	$^1/_4$	0.59406(10)	0.00557(18)
P2	0.12981(8)	$^1/_4$	0.24431(10)	0.00562(17)
P3	0.37815(8)	$^1/_4$	0.42199(9)	0.00540(18)
$DyMnCu_4P_3$				
Dy	0.29123(2)	$^1/_4$	0.92067(2)	0.00506(8)
Mn	0.01841(6)	$^1/_4$	0.79074(7)	0.01228(15)
Cu1	0.00497(4)	$^1/_4$	0.41102(5)	0.00727(12)
Cu2	0.06443(4)	$^1/_4$	0.03997(5)	0.00667(12)
Cu3	0.30531(4)	$^1/_4$	0.62922(5)	0.00709(12)
Cu4	0.32149(5)	$^1/_4$	0.21631(5)	0.00697(11)
P1	0.11606(9)	$^1/_4$	0.59359(10)	0.00500(19)
P2	0.12967(8)	$^1/_4$	0.24496(10)	0.00495(18)
P3	0.37780(9)	$^1/_4$	0.42193(9)	0.00486(19)
$HoMnCu_4P_3$				
Ho	0.29110(2)	$^1/_4$	0.92089(2)	0.00643(5)
Mn	0.01874(6)	$^1/_4$	0.78984(7)	0.01396(13)
Cu1	0.00493(4)	$^1/_4$	0.41148(5)	0.00867(10)
Cu2	0.06436(4)	$^1/_4$	0.04035(5)	0.00808(10)
Cu3	0.30550(4)	$^1/_4$	0.62948(5)	0.00841(10)
Cu4	0.32111(4)	$^1/_4$	0.21632(5)	0.00839(10)
P1	0.11648(8)	$^1/_4$	0.59317(10)	0.00637(17)
P2	0.12968(8)	$^1/_4$	0.24582(10)	0.00657(17)
P3	0.37753(8)	$^1/_4$	0.42185(10)	0.00637(17)

[a]All atoms in Wyckoff position 4c. [b]U_{eq} is defined as one-third of the trace of the orthogonalized U_{ij} tensor.

Table 3. Interatomic Distances (Å) for $REMnCu_4P_3$ (RE = Gd−Ho)

	$GdMnCu_4P_3$	$TbMnCu_4P_3$	$DyMnCu_4P_3$	$HoMnCu_4P_3$
RE−P3 (×2)	2.8783(9)	2.8642(8)	2.8550(9)	2.8484(8)
RE−P2 (×2)	2.8913(9)	2.8761(8)	2.8683(9)	2.8609(8)
RE−P1 (×2)	2.9409(9)	2.9233(8)	2.9132(8)	2.9038(8)
Mn−P1	2.4661(13)	2.4666(13)	2.4731(13)	2.4684(13)
Mn−P2 (×2)	2.7001(10)	2.6950(9)	2.6904(9)	2.6904(9)
Mn−P3 (×2)	2.7156(10)	2.7121(9)	2.7086(10)	2.7095(9)
Cu1−P2	2.4129(12)	2.4027(12)	2.3969(12)	2.3934(12)
Cu1−P1 (×2)	2.4387(8)	2.4357(8)	2.4343(8)	2.4341(7)
Cu1−P1	2.4443(12)	2.4355(12)	2.4313(12)	2.4263(12)
Cu2−P2	2.3710(13)	2.3752(12)	2.3758(12)	2.3801(12)
Cu2−P3	2.3892(12)	2.3922(12)	2.3966(12)	2.3987(12)
Cu2−P3 (×2)	2.4048(8)	2.4020(7)	2.3999(7)	2.4003(7)
Cu3−P2 (×2)	2.4195(8)	2.4173(8)	2.4163(8)	2.4152(8)
Cu3−P1	2.4377(13)	2.4311(12)	2.4249(13)	2.4232(12)
Cu3−P3	2.4380(12)	2.4341(12)	2.4322(12)	2.4325(12)
Cu4−P3	2.3521(12)	2.3486(12)	2.3455(11)	2.3439(12)
Cu4−P2	2.4501(12)	2.4472(12)	2.4461(12)	2.4426(12)
Cu4−P1 (×2)	2.4541(8)	2.4490(7)	2.4460(8)	2.4446(7)
Mn−Cu2	2.7626(11)	2.7698(12)	2.7705(10)	2.7189(9)
Mn−Cu3	2.8345(11)	2.8335(10)	2.8323(10)	2.8361(9)
Mn−Cu2 (×2)	2.8504(8)	2.8465(7)	2.8395(7)	2.8410(7)
Mn−Cu4 (×2)	2.8982(8)	2.8895(7)	2.8871(7)	2.8818(7)
Mn−Cu1 (×2)	2.9236(8)	2.9137(7)	2.9113(7)	2.9045(7)
Cu1−Cu4	2.6993(9)	2.6999(8)	2.7020(8)	2.7080(8)
Cu1−Cu1 (×2)	2.7335(8)	2.7171(8)	2.7085(8)	2.6978(8)
Cu2−Cu2 (×2)	2.6486(8)	2.6445(7)	2.6441(8)	2.6426(7)
Cu2−Cu3 (×2)	2.7071(6)	2.6962(5)	2.6899(6)	2.6852(5)
Cu3−Cu4 (×2)	2.6714(6)	2.6616(5)	2.6548(6)	2.6493(5)

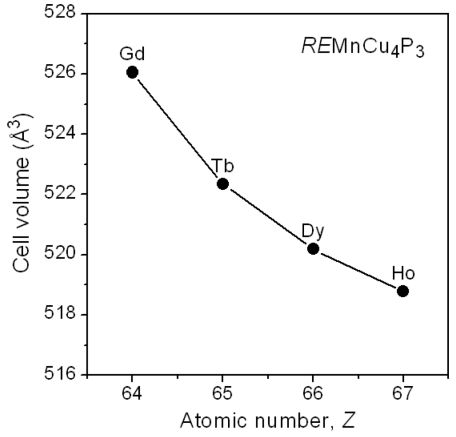

Figure 1. Plot of unit cell volumes for $REMnCu_4P_3$ (RE = Gd−Ho).

$Zr_2Fe_{12}P_7$-type phases given their similar compositions.[10] A quaternary silicide $Y(Rh_{0.42}Ni_{0.58})Ni_4Si_3$ adopts the unrelated orthorhombic YNi_5Si_3-type structure[24] but exhibits partial ordering of Rh and Ni atoms, in contrast to the essentially complete ordering of Mn and Cu atoms observed in $REMnCu_4P_3$ here.

In the structure of $REMnCu_4P_3$, all P atoms are located within the centers of trigonal prisms with metal atoms at the vertices; this coordination geometry is augmented by three further metal atoms capping the rectangular faces of the trigonal prisms to give CN9 (Figure 2). The P-centered trigonal prisms are arranged in groups of three sharing a common RE−RE edge, forming propellor-shaped units. The trigonal prisms extend as confacial columns along the *b* direction, and the propellor-shaped units are connected in a zigzag manner along the *a* direction, resulting in corrugated layers parallel to the *ab* plane. (In the related orthorhombic $LaCo_5P_3$- and UNi_5Si_3-type structures, similar propellor-shaped units are also present, but they are connected in different ways.[13]) All atoms are located at either $y = {}^1/_4$ or ${}^3/_4$, such that these layers are alternately displaced as they stack along the *c* direction. Within the five transition-metal sites, Mn atoms occupy the larger one coordinated by P atoms in a square-pyramidal geometry (CN5; 2.47−2.72 Å) and Cu atoms

dx.doi.org/10.1021/ic502075x | Inorg. Chem. 2015, 54, 860−866

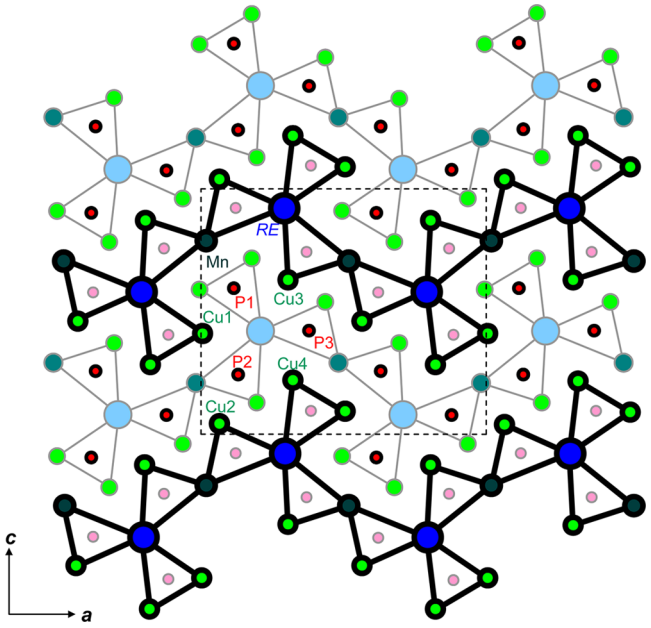

Figure 2. Structure of $REMnCu_4P_3$ (RE = Gd−Ho) built up of propellor-shaped units of trigonal prisms with P atoms (red) at the centers and RE (blue), Mn (dark cyan), and Cu atoms (green) at vertices. Thick and thin lines distinguish between atoms displaced by half of the *b* parameter.

occupy the remaining four coordinated in a tetrahedral geometry (CN4; 2.34−2.45 Å; Figure S1 in the SI). There is no tendency for site mixing, as confirmed by the structural refinements and by the inability to prepare other members of the hypothetical solid solutions $RE(Mn_xCu_{1-x})_5P_3$.

An alternate way to describe the structure is to focus on large triangular assemblies "AB_6C_3" (where A = RE, B = Mn/Cu, and C = P);[3] this approach draws attention to the close relationship between the orthorhombic YCo_5P_3-type structure adopted by $REMnCu_4P_3$ and the hexagonal $Zr_2Fe_{12}P_7$-type structure adopted by $RE_2Mn_3Cu_9P_7$ (Figure 3). The six B atoms lie at the corners of four smaller triangles. In $REMnCu_4P_3$, two corners of the large triangular assemblies are Cu atoms and are shared with adjacent assemblies, giving the formula $AB_4B_{2/2}C_3$ or AB_5C_3 corresponding to the YCo_5P_3-type structure. In $RE_2Mn_3Cu_9P_7$, all three corners of the large triangular assemblies are Mn atoms, which are not shared with adjacent assemblies; the unit cell contains two of these assemblies and one isolated P atom (located along the *c* axis), giving the formula $2AB_6C_3$ + C or $A_2B_{12}C_7$ corresponding to the $Zr_2Fe_{12}P_7$-type structure. These two descriptive schemes, the first based on coordination polyhedra and the second based on triangular assemblies, are valuable for systematizing a large number of structures of many metal-rich pnictides and for predicting new ones.[1−3]

The extent of RE substitution in the orthorhombic $REMnCu_4P_3$ series is restricted to smaller RE atoms (Gd−Ho), in contrast to the hexagonal $RE_2Mn_3Cu_9P_7$ series, which forms for larger RE atoms (La−Nd, Sm, and Gd−Dy) and can be extended to the arsenides $RE_2Mn_3Cu_9As_7$ (RE = La−Nd).[8] The RE atoms are coordinated identically in both structures by P atoms in a trigonal-prismatic geometry (CN6). However, if Cu atoms (within ∼3.3 Å) are included in the coordination sphere, the unique RE atom has CN16 in $REMnCu_4P_3$, whereas the two RE atoms have CN15 and CN18 in $RE_2Mn_3Cu_9P_7$.

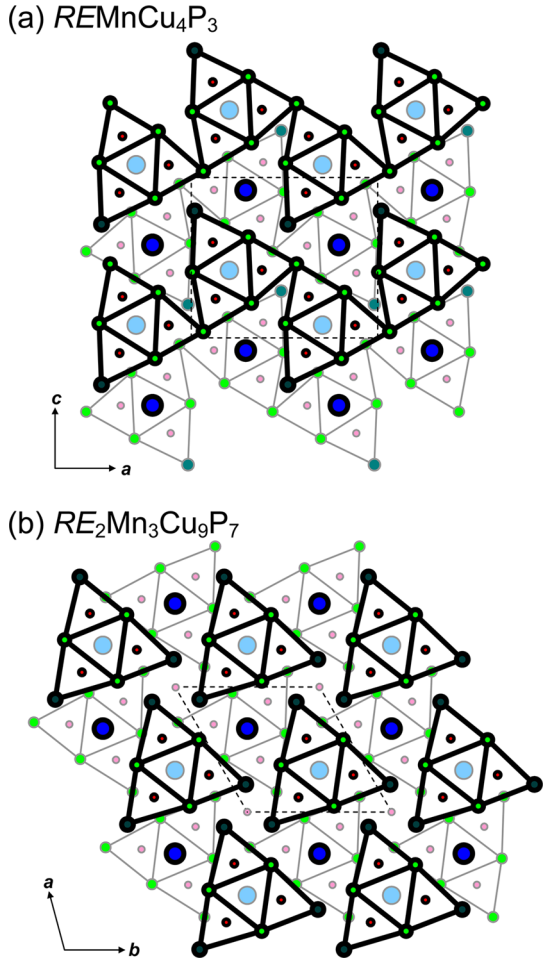

Figure 3. Comparison of (a) $REMnCu_4P_3$ (RE = Gd−Ho; ordered YCo_5P_3-type) and (b) $RE_2Mn_3Cu_9P_7$ (RE = La−Nd, Sm, and Gd−Dy; ordered $Zr_2Fe_{12}P_7$-type) structures, built up of triangular assemblies AB_6C_3 as proposed by Pivan et al.[3] Thick and thin lines distinguish between atoms displaced by half of the cell parameter along the viewing direction.

The distinction is subtle, but evidently the formation of $RE_2Mn_3Cu_9P_7$ with larger RE atoms is consistent with the presence of the higher CN18 site. In general, compounds with the YCo_5P_3-type structure tend to be found with smaller RE atoms, although there are a few exceptions.[10,13,15−19]

The quaternary phosphides are formally charge-balanced as $RE^{3+}Mn^{2+}(Cu^{+})_4(P^{3-})_3$ and thus conform to a generalized relationship, followed by many other metal-rich pnictides M_2Pn, between valences and site occupations of the metal atoms: 3+ in trigonal prisms (CN6), 2+ in square pyramids (CN5), 1+ in tetrahedra (CN4), and 0 in trigonal planes (CN3).[2,25] Bond-valence-sum (BVS) calculations[26] are useful to further evaluate the propensity for the one CN5 and four CN4 sites to be occupied by Mn versus Cu atoms. If Mn atoms are placed in these sites, the BVSs are 1.69 in the CN5 site and 2.45−2.63 in the CN4 sites; conversely, if Cu atoms are placed in these sites, the BVSs are 0.82 in the CN5 site and 1.18−1.27 in the CN4 sites. In other words, the Mn atoms are slightly underbonded in the CN5 site but severely overbonded in the CN4 sites. If we accept at face value that the CN5 site really prefers a divalent metal atom, then Cu atoms would be severely underbonded in the CN5 site but only slightly overbonded in the CN4 sites; of course, divalent Cu atoms are highly unlikely

dx.doi.org/10.1021/ic502075x | *Inorg. Chem.* 2015, 54, 860−866

to occur in pnictides. This BVS analysis accounts neatly for coordination preferences. However, even a rudimentary analysis based on Pauling's electroneutrality principle[27] reveals that the sum of electrostatic bond strengths of the surrounding metal atoms (2.9−3.0) compensates exactly for the valence of each of the P atoms; any exchange of the Mn and Cu atoms within the CN5 versus CN4 sites only exacerbates deviations from electroneutrality.

It is tempting to suggest that simple electronic factors also dictate formation of the YCo_5P_3-type structure, such as the valence electron count (vec). Previously known ternary rare-earth phosphides REM_5P_3 adopting this structure were limited to M = Fe and Co,[10,13,15] with vec = 58 and 63, respectively. Then, the existence of $REMnCu_4P_3$ (vec = 69) could be attributed to a tendency to lower the electron count relative to $RECu_5P_3$ (vec = 73), which is unknown. However, this analysis cannot account for the absence of $RENi_5P_3$ (vec = 68). To a first approximation, the band structure of $REMnCu_4P_3$ might be thought to be intermediate between $RECo_5P_3$ and $RECu_5P_3$, with the Fermi level simply shifted as a result of a change in the electron count. Band-structure calculations were carried out on model compounds containing Y, a nonmagnetic RE component. The density of states (DOS) curves for YCo_5P_3 and hypothetical YCu_5P_3 do share similar features, broadly speaking (Figure S2 in the SI). However, the presence of two different types of transition metals has profound effects on the band structure of $YMnCu_4P_3$, which cannot be predicted on the basis of a rigid band approximation. The simple formulation $RE^{3+}Mn^{2+}(Cu^{+})_4(P^{3-})_3$ is correctly reflected by the occurrence of mostly empty Y states found above the Fermi level, partly filled Mn 3d states (−1 to +1 eV), mostly filled Cu 3d states (the large peak straddling −4 eV), and filled P 3p (−7 to −1 eV) and 3s states (−12 eV, not shown) in the DOS curve (Figure 4a). Lowering the Fermi level in YCu_5P_3 does not reproduce the DOS curve of $YMnCu_4P_3$ because the higher-lying and partly filled Mn 3d states in $YMnCu_4P_3$ are actually pinned to the Fermi level. Bonding interactions between transition-metal and P atoms are nearly optimized, as seen by the occupation of all bonding levels in the crystal orbital Hamilton population (COHP) curves (Figure 4b), which results in large integrated COHP values of 1.38 eV/bond for Mn−P contacts and 1.59 eV/bond for Cu−P contacts. Weaker Y−P (0.74 eV/bond) and metal−metal (Mn−Cu, 0.41 eV/bond; Cu−Cu, 0.49 eV/bond) interactions supplement the bonding stability of the structure.

The presence of substantial Mn-based states near the Fermi level suggests that there should be a tendency for polarization that will lead to a decrease in the DOS at the Fermi level. Spin-polarized calculations on both ferromagnetic and antiferromagnetic models, ordered along the *b* direction, revealed that the Mn 3d states become split by ∼3 eV, reflecting strong polarization (Figure 5). Both models are lower in energy than the nonmagnetic structure by essentially the same amount (3.0 eV) and with similar magnetic moments of 3.6 μ_B/formula unit originating from the Mn atoms, so it is not possible to determine which will be the magnetic ground state until experimental measurements are performed. At the Fermi level, the DOS is small but nonzero for the ferromagnetic model and it is negligible for the antiferromagnetic model, indicating that the electrical conductivity is poor in either scenario. The shortest Mn−Mn distances are 3.8 Å, corresponding to the *b* parameter, which are too long for direct interactions between spins; the most likely mechanism thus involves indirect

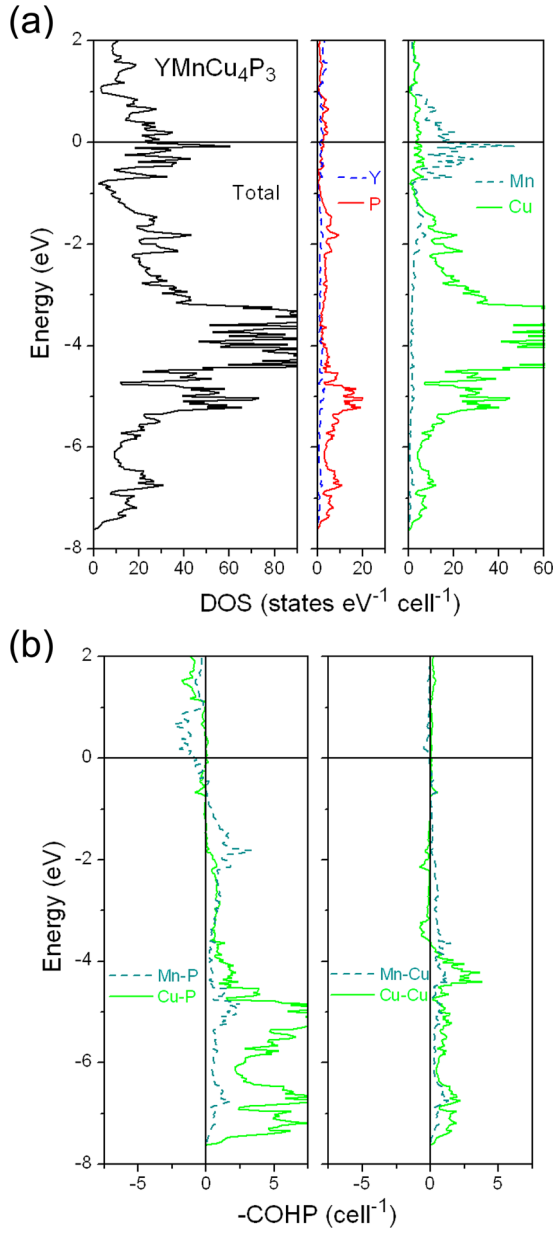

Figure 4. (a) DOS and its atomic projections for $YMnCu_4P_3$. (b) COHP curves for Mn−P, Cu−P, Mn−Cu, and Cu−Cu interactions. The Fermi level is at 0 eV.

interactions mediated through the conduction electrons (RKKY interactions) in the ferromagnetic model or coupling via the P atoms in the antiferromagnetic model.

The electrical resistivity for a single crystal of $TbMnCu_4P_3$ was measured (Figure 6). The relatively high values of the resistivity (ρ_{300} = ∼110 $\mu\Omega$·cm) and the weak temperature dependence suggest a poor metal, consistent with the band-structure calculations. There is a distinct change in curvature below ∼100 K, which is probably associated with the loss of spin-disorder scattering below a magnetic ordering transition. Further work is in progress to prepare phase-pure samples of $REMnCu_4P_3$ to measure their magnetic properties.

CONCLUSIONS

Cation ordering appears to be a viable strategy to introduce further complexity in metal-rich pnictides M_2Pn, which can be

dx.doi.org/10.1021/ic502075x | Inorg. Chem. 2015, 54, 860−866

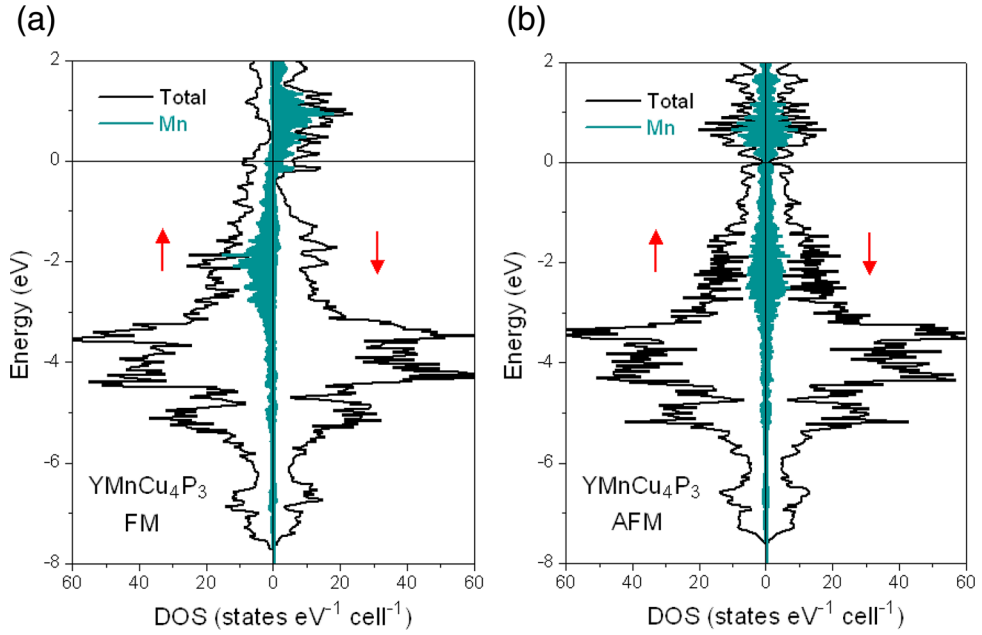

Figure 5. DOS curves for spin-polarized $YMnCu_4P_3$ models with (a) ferromagnetic and (b) antiferromagnetic arrangements of Mn spins. Contributions from Mn states are identified by the shaded region.

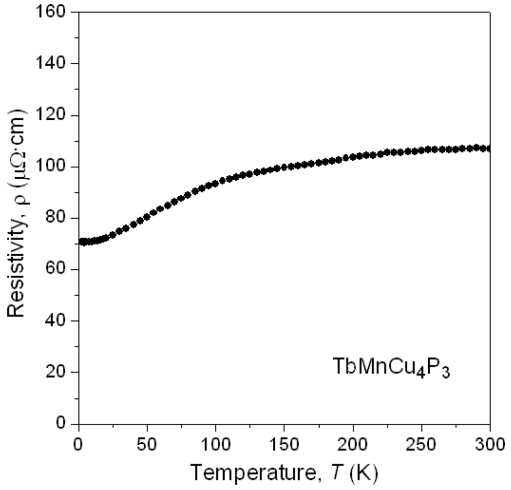

Figure 6. Plot of the electrical resistivity versus temperature for $TbMnCu_4P_3$.

readily extended to ternary and now quaternary phases, as demonstrated here. It might even be possible to prepare quinary phases, if all four types of metal sites (with coordination geometries ranging from CN6 to CN3) are occupied by different atoms. Notwithstanding the apparent adherence to charge-balanced formulations, many of these phases lack a band gap in their electronic structure because of the presence of partly filled d bands of transition-metal components such as Mn. The physical properties of these ternary and quaternary phases remain underexplored and deserve further investigation.

■ ASSOCIATED CONTENT

Supporting Information

X-ray crystallographic files in CIF format, full crystallographic details, EDX analyses, coordination geometries, and additional band-structure calculations. This material is available free of charge via the Internet at http://pubs.acs.org. Additional CIF files may be obtained from Fachinformationszentrum Karlsruhe, Abteilung PROKA, 76344 Eggenstein-Leopoldshafen, Germany (CSD 428286−428289).

■ AUTHOR INFORMATION

Corresponding Author

*E-mail: arthur.mar@ualberta.ca.

Notes

The authors declare no competing financial interest.

■ ACKNOWLEDGMENTS

This work was supported by the Natural Sciences and Engineering Research Council of Canada.

■ REFERENCES

(1) Gladyshevskii, E. I.; Grin, Yu. N. *Kristallografiya* **1981**, *26*, 1204−1214.
(2) Madar, R.; Ghetta, V.; Dhahri, E.; Chaudouet, P.; Senateur, J. P. *J. Solid State Chem.* **1987**, *66*, 73−85.
(3) Pivan, J.-Y.; Guérin, R.; Sergent, M. *J. Solid State Chem.* **1987**, *68*, 11−21.
(4) Oyama, S. T.; Gott, T.; Zhao, H.; Lee, Y.-K. *Catal. Today* **2009**, *143*, 94−107.
(5) Prins, R.; Bussell, M. E. *Catal. Lett.* **2012**, *142*, 1413−1436.
(6) Maple, M. B.; Hamlin, J. J.; Zocco, D. A.; Janoschek, M.; Baumbach, R. E.; White, B. D.; Fisher, I. R.; Chu, J.-H. *EPJ Web Conf.* **2012**, *23*, 00012−1−00012−8.
(7) Dhahri, E. *J. Phys.: Condens. Matter* **1996**, *8*, 4351−4360.
(8) Stoyko, S. S.; Ramachandran, K. K.; Mullen, C. S.; Mar, A. *Inorg. Chem.* **2013**, *52*, 1040−1046.
(9) El Ghadraoui, E. H.; Pivan, J.-Y.; Guérin, R. *J. Solid State Chem.* **1989**, *78*, 262−270.
(10) Jeitschko, W.; Meisen, U.; Scholz, U. D. *J. Solid State Chem.* **1984**, *55*, 331−336.
(11) Sheldrick, G. M. *SHELXTL*, version 6.12; Bruker AXS Inc.: Madison, WI, 2001.
(12) Gelato, L. M.; Parthé, E. *J. Appl. Crystallogr.* **1987**, *20*, 139−143.
(13) Meisen, U.; Jeitschko, W. *J. Less-Common Met.* **1984**, *102*, 127−134.

(14) Tank, R.; Jepsen, O.; Burkhardt, A.; Andersen, O. K. *TB-LMTO-ASA Program*, version 4.7; Max Planck Institut für Festkörperforschung: Stuttgart, Germany, 1998.
(15) Jeitschko, W.; Reinbold, E. J. *Z. Naturforsch., B: Anorg. Chem., Org. Chem.* **1985**, *40*, 900−905.
(16) Jakubowski-Ripke, U.; Jeitschko, W. *J. Less-Common Met.* **1988**, *136*, 261−270.
(17) Jeitschko, W.; Brink, R.; Pollmeier, P. G. *Z. Naturforsch., B: J. Chem. Sci.* **1993**, *48*, 52−57.
(18) Albering, J. H.; Jeitschko, W. *J. Solid State Chem.* **1995**, *117*, 80−87.
(19) Thompson, C. M.; Kovnir, K.; Zhou, H.; Shatruk, M. *Z. Anorg. Allg. Chem.* **2011**, *637*, 2013−2017.
(20) Stoyko, S.; Oryshchyn, S. V. *Collect. Abs. 9th Int. Conf. Cryst. Chem. Intermet. Compd. (Lviv)* **2005**, *58*.
(21) Venturini, G.; Malaman, B. *J. Alloys Compd.* **1997**, *261*, 19−25.
(22) Li, B.; Corbett, J. D. *Inorg. Chem.* **2007**, *46*, 2237−2242.
(23) Hoffmann, R.-D.; Pöttgen, R. *Z. Anorg. Allg. Chem.* **1999**, *625*, 994−1000.
(24) Zhao, J. T.; Mao, S. Y. *Xiamen Daxue Xuebao, Ziran Kexueban* **1998**, *37*, 537−541.
(25) Zhao, J. T.; Chabot, B.; Parthé, E. *Acta Crystallogr., Sect. C* **1987**, *43*, 1458−1461.
(26) Brese, N. E.; O'Keeffe, M. *Acta Crystallogr., Sect. B* **1991**, *47*, 192−197.
(27) Pauling, L. *The Nature of the Chemical Bond*, 3rd ed.; Cornell University Press: Ithaca, NY, 1960.